PHYSICAL REVIEW D **95,** 124017 (2017)

Dark SU(N) glueball stars on fluid branes

Roldão da Rocha*

Centro de Matemática, Computação e Cognição,
Universidade Federal do ABC—UFABC 09210-580 Santo André, Brazil

(Received 4 January 2017; revised manuscript received 18 April 2017; published 8 June 2017)

The glueball dark matter, in the pure SU(N) Yang-Mills theory, engenders dark SU(N) stars that comprise self-gravitating compact configurations of scalar glueball fields. Corrections to the highest frequency of gravitational wave radiation emitted by dark SU(N) star mergers on a fluid brane with variable tension, implemented by the minimal geometric deformation, are derived, and their consequences are analyzed. Hence, dark SU(N) star mergers on a fluid braneworld are shown to be better detectable by the LIGO and the eLISA experiments.

DOI: 10.1103/PhysRevD.95.124017

I. INTRODUCTION

Dark matter and dark energy comprise new directions in gravity and high-energy physics, toward theories that are beyond General Relativity (GR) and that can explain two such puzzling phenomena. Among successful attempts to propose theories beyond GR, the method of geometrical deformation (MGD) consists of a suitable approach to derive new solutions of the effective Einstein field equations [1–3], encoding compact stellar distributions. These new solutions are complementary to other successful paradigms [4–6]. The MGD comprises the brane tension (σ) as a free parameter, controlling the high-energy regime of an inflationary braneworld scenario that has the GR as the low-energy limit. In fact, during the cosmological evolution, the brane temperature has been severely modified. It varied from, for instance, $T \sim 10^4$ K—when the matter density equaled the radiation density, around 5.6×10^3 yr after the big bang—to the current value of $T \sim 2.73$ K, in the cosmic microwave background (CMB). An underlying setup can thus be implemented by a variable tension fluid brane [7], whereon compact self-gravitating systems can undergo the MGD [8].

The MGD was developed using Randall-Sundrum–like models [4,9]. It has the bulk dark pressure and radiation as leading constituents of the stress-energy tensor, in the brane effective Einstein field equations [10]. Explicit solutions are compact stellar structures with a bulk Weyl fluid imprint [1–3,11]. The MGD is a strong and robust procedure that has been recently endowed with observational and experimental precise bounds, from gravitational lensing effects [12] to the classical tests of GR [13].

On the other hand, gauge fields that are further away from the Standard Model of elementary particles were proposed as pure Yang-Mills dark fields [14,15]. In fact, the Standard Model can be coupled to hidden sectors, governed by a pure Yang-Mills setup, in the low-energy regime. The scalar glueball dark matter model implements such a SU(N) Yang-Mills sector [14,16,17], as a self-interacting field with a large cross section. When Standard Model particles and fields are forbidden to interact with the SU(N) scalar glueball, gravity can induce a self-gravitating system, manifesting Bose-Einstein condensation of glueballs into compact stellar objects. Reference [16] discusses relevant elastic scatterings among glueballs, manifesting their feasibility as a self-interacting dark matter candidate. A refined and detailed analysis can be checked in Ref. [14], together with other general aspects [18].

Although dark SU(N) compact systems were studied [16], any realistic approach that provides observational and experimental signatures of dark SU(N) stars on inflationary scenarios is still lacking. Here, the MGD is proposed as a procedure to implement dark SU(N) braneworld stars, in the context of the evolution of the Universe, as well as to refine the analysis of gravitational waves produced by dark SU(N) glueball star mergers, enhancing the window for current experiments to detect them.

This paper is organized as follows. Section II is devoted to a brief review, regarding the MGD of stellar distributions on a fluid brane, ruled by a variable tension that encodes the cosmological evolution. In Sec. III, corrections to the highest frequency of gravitational wave radiation, emitted by dark SU(N) star mergers due to the finite brane tension, are derived for both the ϕ^4 self-interacting glueball potential and the glueball potential in the large N limit. These corrections make the gravitational wave radiation, emitted by dark SU(N) MGD star mergers, easier to detect than in the GR limit setup. Hence, a larger spectrum of gravitational waves on fluid branes is expected, enhancing the window to be probed by the LIGO and the eLISA experiments. Section IV is dedicated to drawing the conclusions and final comments.

II. MGD SETUP AND FLUID BRANES

The MGD procedure is able to derive high-energy corrections to GR, when the vacuum in the outer region of a

*roldao.rocha@ufabc.edu.br

compact distribution is permeated by a five-dimensional (5D) bulk Weyl fluid [1,3,19]. The codimension-1 brane that designates our Universe has tension (self-gravity) as a leading parameter, which varies as the temperature decreases, across the Universe inflation [7,20]. The most useful and applicable braneworld scenarios in this context are implemented by fluid branes, evincing the Eötvös law that provides the dependence of the brane tension with the temperature [7,20].

The MGD setup has recently imposed the brane (variable) tension bounds $\sigma \gtrsim 5.19 \times 10^6$ MeV^4 (in the context of the classical tests of GR) [13] and $\sigma \gtrsim 3.18 \times 10^6$ MeV^4 (regarding the Bose-Einstein condensation of weakly interacting gravitons into MGD black holes) [21]. The MGD represents a deformation of the Schwarzschild metric, implemented by bulk effects in the braneworld paradigm, the low energy regime $\sigma \to \infty$ of which recovers the Schwarzschild standard solution.

The four-dimensional (4D) Einstein effective equations can be derived when the 5D bulk Einstein equations are projected onto the 4D brane, by the Gauss-Codazzi method (the convention $8\pi G = c = 1 = \hbar$ is going to be fixed,[1] where $G = \hbar c/M_{\rm pl}^2$ and $M_{\rm pl}$ denotes the Planck scale, and $\mu, \nu = 0, 1, 2, 3$), yielding [10]

$$R_{\mu\nu} + \left(\Lambda - \frac{1}{2}R\right) g_{\mu\nu} - \mathrm{T}_{\mu\nu} = 0, \tag{1}$$

where $R_{\mu\nu}$, R, and Λ are, respectively, the Ricci tensor, the Ricci scalar, and the 4D cosmological constant. The effective stress tensor in Eq. (1) can be split into a sum, $\mathrm{T}_{\mu\nu} = T_{\mu\nu} + \mathcal{E}_{\mu\nu} + \sigma^{-1} S_{\mu\nu}$, where the first component $T_{\mu\nu}$ denotes the brane matter stress tensor and $\mathcal{E}_{\mu\nu}$ inscribes high-energetic corrections from the 5D Weyl fluid. The tensor $S_{\mu\nu}$ encrypts Kaluza-Klein imprints from the bulk onto the brane [4,10].

Compact stellar structures that are solutions of the Einstein brane field equations (1) are usually obtained for static, spherically symmetric, metrics (2),

$$ds^2 = -A(r)dt^2 + (B(r))^{-1}dr^2 + r^2(d\vartheta^2 + \sin^2\vartheta d\varphi^2). \tag{2}$$

The MGD procedure fixes the g_{tt} metric component in (2) and deforms the outer $g_{rr}^{-1} \equiv B(r)$ metric component [2,3,11],

$$B(r) = 1 - \frac{2M}{r} + \varsigma \exp\left(\int_{\rm R}^{r} \frac{f(A(\mathrm{r}))}{g(A(\mathrm{r}))} d\mathrm{r}\right), \tag{3}$$

where $f(A(r)) \equiv \frac{AA''}{A'^2} + (\ln(A))'^2 + \frac{2}{r}\ln(A)' - 1 + \frac{1}{r^2}$ and $g^{-1}(A(r)) = \frac{1}{2}\ln(A)' + \frac{2}{r}$ [2], $()' \equiv \frac{d()}{dr}$, and $\mathrm{R} \equiv \int r^3\rho(r)dr / \int r^2\rho(r)dr$, where ρ is the energy density of the stellar matter distribution [1]. The parameter ς in Eq. (3) encodes a bulk-induced deformation of the vacuum, at the compact distribution surface, comprising the necessary 5D (bulk) Weyl fluid data onto the brane [13]. It is significant to observe that the outer metric is defined in the region $r > \mathrm{R}$ [1], the deformation of which yields [2]

$$A(r) = 1 - \frac{2M}{r}, \tag{4a}$$

$$B(r) = \left[1 + \left(1 - \frac{3M}{2r}\right)^{-1} \varsigma \frac{\mathfrak{I}}{r}\right]\left(1 - \frac{2M}{r}\right), \tag{4b}$$

where

$$\mathfrak{I} \equiv \left(1 - \frac{2M}{\mathrm{R}}\right)^{-1}\left(1 - \frac{3M}{2\mathrm{R}}\right)\mathrm{R}. \tag{5}$$

The MGD black hole event horizons are $r_1 = 2M$ and $r_2 = -\varsigma\mathfrak{I} + \frac{3M}{2}$. The infinitely rigid brane limit $\varsigma^{-1} \sim \sigma \to \infty$, which characterizes the GR limit, yields $r_1 > r_2$. Besides, ς is a parameter that relies on the inherent compact star configuration. References [1,8] show that the metric radial component (4a) can be written as

$$B(r) = 1 - \frac{2M}{r} - \left(1 - \frac{2M_0}{r}\right)\left(1 - \frac{3M_0}{2r}\right)^{-1}\frac{\mathfrak{I}_0\varsigma}{r}, \tag{6}$$

thus exhibiting a part that is beyond the Schwarzschild solution, up to order $\mathcal{O}(\sigma^{-2})$, where $M_0 = M|_{\sigma\to\infty}$ is the GR mass function and $\mathfrak{I}_0 = \mathfrak{I}(M_0)$, concerning Eq. (5). Bulk imprints are highest at the star surface $r = \mathrm{R}$. This shall be a prominent information in the analysis of dark SU(N) stars on fluid branes, in the next section.

The less compact the star, the smaller the $|\varsigma|$ parameter is [1,2]. Moreover, the current experimental and observational data were used in Ref. [13] to impose the strongest bound $|\varsigma| \lesssim 6.1 \times 10^{-11}$ on the MGD parameter, using the classical tests of GR. This result, together with the most recent and strict bound on the variable brane tension $\sigma \gtrsim 3.18 \times 10^6$ MeV^4 [21], justifies high-order $\mathcal{O}(\sigma^{-2})$ terms to be dismissed, yielding

$$\varsigma(\sigma, \mathrm{R}) = -\frac{b_0}{\mathrm{R}^2}\sigma^{-1}, \tag{7}$$

where $b_0 \sim 1.35$ [13]. The negativeness of ς compels the MGD star gravitational field to be weakened, as an effect of a finite brane tension, when compared to the GR regime $\sigma \to \infty$.

Heretofore, no condition on the variable brane tension has been imposed, although cosmological evidence drives the brane tension to fluctuate across the Universe inflation [7,22]. On Eötvös fluid branes, the brane tension varies with respect to the Universe temperature T. One associates

[1]Obviously, the precise values of all involved parameters shall be suitably taken into account, in the calculations in Sec. III.

the regime $\sigma \approx T - \tau$ [7], where τ is some critical value that makes σ to assume only non-negative values after the big bang [7,20]. This varying brane tension can eliminate any initial singularity at the early Universe. In fact, the brane Universe was created at a τ temperature, corresponding to the scale factor value a_0 that is defined by the coupling constants [7,22]. Reference [7] derived the relationship between temperature and the scale factor, $T(t) \approx \frac{1}{a(t)}$ [7]. This result yields a time-dependent brane tension,

$$\frac{\sigma(t)}{\sigma_0} = 1 - \frac{a_0}{a(t)}. \tag{8}$$

At the extremely hot early Universe, the brane tension was negligible ($\sigma \approxeq 0$). Subsequently, both the variable brane tension and the 4D coupling parameter grew, as the scale factor asymptotically increased, in the inflationary braneworld scenario [23]. The time-dependent brane tension expression yields $\frac{\Lambda_{4D}}{\Lambda_0} = 1 - \frac{a_0}{a(t)}\left(1 - \frac{a_0}{a(t)}\right)$. This (dynamical) cosmological "constant" had attained a huge negative value and achieved small positive values [20]. It also engendered supplementary attraction (repulsion) at small (large) values of the scale factor, similarly to the dark matter (dark energy). This inflationary cosmology scenario emulates the (cosmological) standard model at late times, wherein the energy that is absorbed by the brane thrusts the 5D bulk toward an anti-de Sitter bulk, as a mere consequence of the highest symmetry [22,24].

In the next section, the dark SU(N) stellar system, constituted by self-interacting scalar glueballs, is studied on a fluid brane, the tension of which obeys the Eötvös law. Corrections to the gravitational waves frequency, emitted by dark SU(N) star mergers on the fluid brane, are then derived as a consequence of the dark SU(N) star mass and radii variation on a fluid brane. Moreover, dark SU(N) stars features can be, in this context, analyzed along the inflationary braneworld era.

III. FLUID BRANE CORRECTIONS TO DARK SU(N) STARS

Hidden SU(N) Yang-Mills sectors, which are farther away than the Standard Model of elementary particles, can be realized by the (scalar) glueball dark matter model [14,16]. The gravitational interactions among glueballs engender a self-interacting system, having the glueball mass (m) and the number (N) of colors as the main underlying parameters. When $10\ \text{eV} \lesssim m \lesssim 10\ \text{KeV}$ and $10^3 \lesssim N \lesssim 10^6$, then the dark glueball field self-gravity takes part, forming dark SU(N) compact stellar distributions [15,16]. To be compatible with the Bose-Einstein condensation of the scalar glueballs into static, spherically, symmetric solutions, the glueball fields are assumed to be periodic, $\phi(r,t) = \Phi(r)\cos\omega t$ [16].

The action for the most general nonlinear interacting scalar field theory reads

$$\mathcal{S} = \int d^4x \left(\frac{1}{2} g^{\mu\nu}\partial_\mu\phi\partial_\nu\phi - V(\phi)\right). \tag{9}$$

The Klein-Gordon equation, which is derived from this action by the Euler-Lagrange equations, couples to the Einstein field equations and shall be analyzed, for both the large N glueball potential and for the ϕ^4 self-interacting glueball potential as well. Hereon, $\dot{(\,)} \equiv \frac{d()}{dt}$.

In the next two subsections, corrections due to the variable brane tension, to the highest frequency of the gravitational wave radiation emitted by SU(N) MGD dark star mergers, shall be analyzed. Such a highest frequency is given, for the Schwarzschild case, by [16] $f_{\max} = \frac{1}{2\pi}\left(\frac{GM}{R^3}\right)^{1/2}$, which can be probed by the LIGO experiment [25]. SU(N) MGD dark stars mergers are, then, shown to provide a better detection of gravitational waves, which is compatible with the current bounds of the brane tension and the CMB, in an inflationary braneworld scenario.

A. Self-interacting ϕ^4 glueball potential

A self-interacting potential for the dark glueball,

$$V(\phi) = \frac{1}{2}m^2\phi^2 + \frac{\lambda}{4!}\phi^4, \tag{10}$$

was shown to rule both the glueball dark matter self-interaction strength and the properties of dark SU(N) stars as well. For $\lambda > 0$, stable dark SU(N) star configurations can be derived, when the repulsive $\lambda\phi^4$ self-interaction compensates gravity [16,26].

The coupled system of Einstein equations and Klein-Gordon ones was derived in Ref. [16]. Imposing time averaging over the oscillation period $\frac{2\pi}{\omega}$ of the ϕ field, such a system yields

$$M'(x) - \left[\frac{\Lambda}{6}\Phi^4(x) + \left(1 + \frac{\Omega^2}{A(x)}\right)\Phi^2(x) + \frac{\Phi'^2(x)}{B(x)}\right]\frac{x^2}{8} = 0, \tag{11a}$$

$$\frac{(\ln A(x))'}{B(x)} + \frac{\Lambda}{48}x\Phi^4(x) + \frac{x}{4}\left(1 - \frac{\Omega^2}{A(x)}\right)\Phi^2(x) - \frac{x}{8}\frac{\Phi'^2(x)}{B(x)} + \frac{1}{x}\left(\frac{1}{B(x)} - 1\right) = 0, \tag{11b}$$

$$\Phi''(x) + \left(\frac{1}{2}\left(\ln\frac{A}{B}\right)' + \frac{2}{x}\right)\Phi'(x) - \left[\frac{\Lambda}{2}\Phi^2(x) + \left(1 - \frac{\Omega^2}{A(x)}\right)\right]B(x)\Phi(x) = 0, \tag{11c}$$

where [16,26]

$$x = mr, \tag{12a}$$

$$\Lambda = \frac{12\lambda}{m^2}, \tag{12b}$$

$$\Omega = \frac{\omega}{m}. \tag{12c}$$

The regime $\Lambda \gg 1$ holds for the glueball dark matter model [27], yielding Eq. (11c) to imply

$$\Lambda^{-1}\left[\phi''(\mathrm{x}) + \left(\frac{2}{\mathrm{x}} + \frac{1}{2}\ln\left(\frac{A}{B}\right)'\right)\phi'(\mathrm{x})\right] - B(\mathrm{x})\phi(\mathrm{x})\left[\left(1 - \frac{\Omega^2}{A(\mathrm{x})}\right) - \frac{1}{2}\phi^2(\mathrm{x})\right] = 0, \tag{13}$$

where

$$\mathrm{x} = \frac{x}{\sqrt{\Lambda}}, \qquad \phi = \sqrt{2\Lambda}\Phi, \qquad \mathrm{M} = \frac{M}{\sqrt{\Lambda}}. \tag{14}$$

The $\Lambda \gg 1$ limit can induce the first term in Eq. (13) to be dismissed, yielding

$$\lim_{\Lambda\gg 1}\left[\phi(\mathrm{x}) - \sqrt{2}\left(\frac{\Omega^2}{A(\mathrm{x})} - 1\right)^{1/2}\right] = 0, \tag{15}$$

implying that

$$\mathrm{M}'(\mathrm{x}) - \mathrm{x}^2\left[\frac{1}{4}\left(\frac{\Omega^2}{B(\mathrm{x})} + 1\right)\phi^2(\mathrm{x}) + \frac{3}{32}\phi^4(\mathrm{x})\right] = 0, \tag{16}$$

$$B(\ln A)'\mathrm{x}^2 - 2\mathrm{M} + \left[\left(1 - \frac{\Omega^2}{A}\right)\frac{\phi^2}{2} + \frac{3}{16}\phi^4\right]\mathrm{x}^3 = 0, \tag{17}$$

where x is the argument of all functions in Eqs. (16) and (17). Similarly to Refs. [16,26], these equations can be solved by numerical methods, with $\mathrm{M}(0) = 0$, for $0 \leq \mathrm{x} \leq x_R$.

The results obtained from using the self-interacting ϕ^4 glueball potential (10) are depicted in Figs. 1–3. In what follows, $\sigma \sim 10^6$ MeV^4 shall denote the current brane tension bound $\sigma \gtrsim 3.18 \times 10^6$ MeV^4 [21]. The same notation shall be used for the values $\sigma \sim 10^9$ and $10^{12} \sim$ MeV^4, but these exact values shall be adopted in what follows, unless otherwise explicitly stated.

The gravitational balance of self-interacting scalar fields was studied [27], also in the context of stability bounds on compact objects [21,28], represented by spherically symmetric boson star solutions. According to the g_{rr}^{-1} metric component in Eq. (4b), the boundary condition $\mathrm{M}(\mathrm{x} = 0) = 0$ implies that $\lim_{\mathrm{M}\to 0} B(r) = 1 + \varsigma\frac{\mathrm{I}}{r}$.

In Fig. 1, the mass spectrum (y axis) between the point $\frac{A(0)}{\Omega^2} = 0$ up to the critical (maximum) point in the

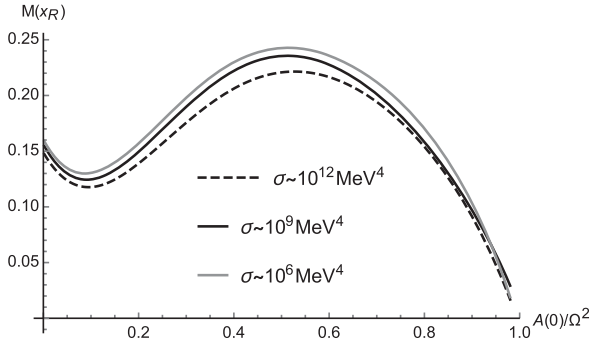

FIG. 1. Dark SU(N) MGD star mass $\mathrm{M}(x_R)$, in the ϕ^4 scalar glueball potential setup, normalized by $\frac{\sqrt{2\lambda}M_{\mathrm{pl}}^3}{m^2}$, with respect to $\frac{A(0)}{\Omega^2}$, for different values of the fluid brane tension $\sigma = 10^{12}$ MeV^4 (dashed line), $\sigma = 10^9$ MeV^4 (black line), and $\sigma \sim 10^6$ MeV^4 (gray line).

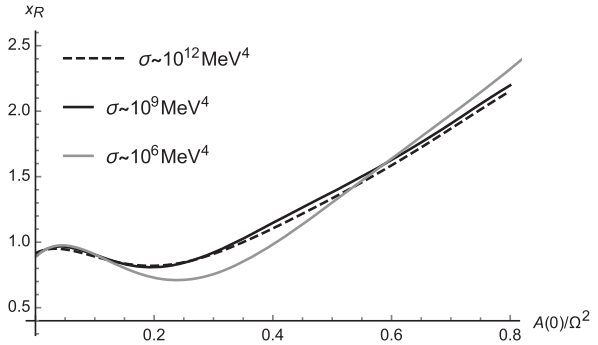

FIG. 2. Dark SU(N) MGD star radius x_R in the ϕ^4 scalar glueball potential setup, normalized by $\frac{\sqrt{2\lambda}M_{\mathrm{pl}}}{m^2}$, with respect to $\frac{A(0)}{\Omega^2}$, for different values of the fluid brane tension $\sigma = 10^{12}$ MeV^4 (dashed line), $\sigma = 10^9$ MeV^4 (black line), and $\sigma = 10^6$ MeV^4 (gray line).

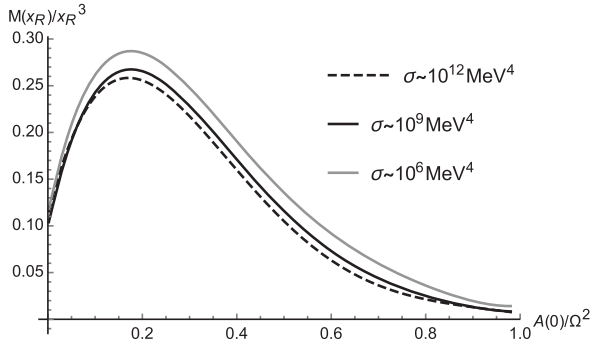

FIG. 3. Dark SU(N) MGD star ratio $\frac{\mathrm{M}(x_R)}{x_R^3}$ in the ϕ^4 scalar glueball potential setup, normalized by $\frac{\sqrt{2\lambda}M_{\mathrm{pl}}}{m^2}$, with respect to $\frac{A(0)}{\Omega^2}$, for different values of the fluid brane tension $\sigma = 10^{12}$ MeV^4 (dashed line), $\sigma = 10^9$ MeV^4 (black line), and $\sigma \sim 10^6$ MeV^4 (gray line).

plots cannot be attained. In fact, Ref. [26] showed that a dark SU(N) star accretes by seizing the surrounding dark matter. Thereafter, the dark SU(N) MGD star mass increases by accretion, up to a maximum, represented in the third column in Table I. The results are presented for different values of the brane tension. Now, the glueball SU(N) dark star has radius and mass that read, respectively [16,26],

$$R = \frac{\sqrt{2\lambda}}{m^2} M_{\rm pl} x_R, \tag{18}$$

$$M = \frac{\sqrt{2\lambda}}{m^2} M_{\rm pl}^3 \mathrm{M}(x_R). \tag{19}$$

Based on the third and fourth columns in Table I, the glueball dark SU(N) MGD star has highest radius and mass, respectively, given by

$$R = \begin{cases} 902.5 m^2\sqrt{\lambda}, & \text{for } \sigma \to \infty \text{ (GR limit)} \\ 929.8 m^2\sqrt{\lambda}, & \text{for } \sigma = 10^{12}\ \text{MeV}^4 \\ 949.2 m^2\sqrt{\lambda}, & \text{for } \sigma = 10^{9}\ \text{MeV}^4 \\ 922.5 m^2\sqrt{\lambda}, & \text{for } \sigma \sim 10^{6}\ \text{MeV}^4 \end{cases} \tag{20}$$

$$M = \begin{cases} \frac{9\sqrt{\lambda}}{m^2} 10^{-2}\ M_\odot, & \text{for } \sigma \to \infty \text{ (GR limit)} \\ \frac{9.04\sqrt{\lambda}}{m^2} 10^{-2}\ M_\odot, & \text{for } \sigma = 10^{12}\ \text{MeV}^4 \\ \frac{9.72\sqrt{\lambda}}{m^2} 10^{-2}\ M_\odot, & \text{for } \sigma = 10^{9}\ \text{MeV}^4 \\ \frac{10.94\sqrt{\lambda}}{m^2} 10^{-2}\ M_\odot, & \text{for } \sigma \sim 10^{6}\ \text{MeV}^4, \end{cases} \tag{21}$$

where $M_\odot$ denotes, as usual, the Solar mass.

Equations (20) and (21), together with the last column of Table I, yield the highest gravitational wave radiation frequency,

$$f_{\rm max} = \frac{m^2\sqrt{\lambda}}{\sqrt{2}\pi M_{\rm pl}} \mathrm{supp}^{1/2}\left(\frac{\mathrm{M}(x_R)}{x_R^3}\right) \approx \beta_1(\sigma)(50\ \text{Hz}), \tag{22}$$

TABLE I. Highest values of the dark SU(N) MGD stars radius (normalized by $\frac{\sqrt{2\lambda}}{m^2} M_{\rm pl}$) and mass (normalized by $\frac{\sqrt{2\lambda}}{m^2} M_{\rm pl}^3$), by accretion, for different values of the fluid brane tension, for a $\lambda\phi^4$ scalar glueball potential.

Brane tension σ	$\frac{A(0)}{\Omega^2}$	Mass $\mathrm{M}(x_R)$	Radius x_R	$\frac{\mathrm{M}(x_R)}{x_R^3}$
∞ (GR limit)	0.533	0.222	1.351	0.090
10^{12} (MeV^4)	0.530	0.223	1.392	0.091
10^{9} (MeV^4)	0.517	0.240	1.421	0.110
10^{6} (MeV^4)	0.509	0.249	1.381	0.142

where the function

$$\beta_1(\sigma) = \mathfrak{a}\sqrt{\lambda}(2m)^2 10^4\ \text{GeV}^{-2} \tag{23}$$

has an adjusting factor $\mathfrak{a}$, which is a function of the variable brane tension, according to Eq. (22) when the last column of Table I is taken into account. Such a factor is given by

$$\mathfrak{a} = \begin{cases} 1, & \text{for } \sigma \to \infty \text{ (GR limit)}, \\ 1.010, & \text{for } \sigma = 10^{12}\ \text{MeV}^4, \\ 1.111, & \text{for } \sigma = 10^{9}\ \text{MeV}^4, \\ 1.262, & \text{for } \sigma \sim 10^{6}\ \text{MeV}^4. \end{cases} \tag{24}$$

The parameter $\mathfrak{a}$ indicates the corrections to the unit (that corresponds to the $\sigma \to \infty$ GR limit), for different values of the brane tension.

The parameter $\mathfrak{a}$ in (24) shows corrections to the highest gravitational wave radiation frequency emitted by dark SU(N) MGD star mergers, due to the brane tension. The current lower bound for the brane tension $\sigma \gtrsim 3.18 \times 10^6$ MeV^4 [21], in the last line of Eq. (24), provides a realistic fluid brane scenario, wherein the highest gravitational wave radiation frequency is up to ~26.2% higher than the predictions in the GR limit.

Now, we can see that the highest gravitational wave frequency that is emitted by dark SU(N) MGD star mergers, in Eqs. (22), for the self-interacting ϕ^4 glueball potential, can be better detected by the LIGO and the eLISA experiments [25], having a wider range than the spectrum of frequencies provided by Schwarzschild solutions [16]. This shall be clear in what follows, by analyzing the N—m parameter space.

Reference [16] argued that the dark SU(N) stars have parameters in the ranges $100\ \text{eV} \lesssim m \lesssim 10\ \text{KeV}$ and $10^3 \lesssim N \lesssim 10^6$, yielding a maximum $10^6\ M_\odot \lesssim M \lesssim 10^9\ M_\odot$ for the dark SU(N) MGD star mass, whereas the lowest dark SU(N) MGD star radius varies in the range $10^2 \lesssim R \lesssim 10^5$, in unit of the Solar radius $R_\odot$. Hence, the highest gravitational wave frequency that is emitted by dark SU(N) MGD stars mergers, given by Eqs. (22), for the ϕ^4 glueball potential (10), can be better detectable by the LIGO and the eLISA experiments [25]. Moreover, dark SU(N) MGD star mergers have specific signatures that are quite different than Schwarzschild black hole mergers, due to the subsequent analysis of Table I, as well as Eqs. (24). In fact, since dark SU(N) MGD stars do not necessarily collapse to form a black hole, their gravitational wave frequency of emission has a distinct signature of the ones emitted by black hole mergers.

The highest frequency of gravitational wave radiation $f_{\rm max}$, emitted from dark SU(N) MGD stellar mergers, can be allocated in the range $30\ \mu\text{Hz} \lesssim f_{\rm max} \lesssim 100$ mHz, which can be further detected by the eLISA mission [29]. In addition, the LIGO experiment can probe the

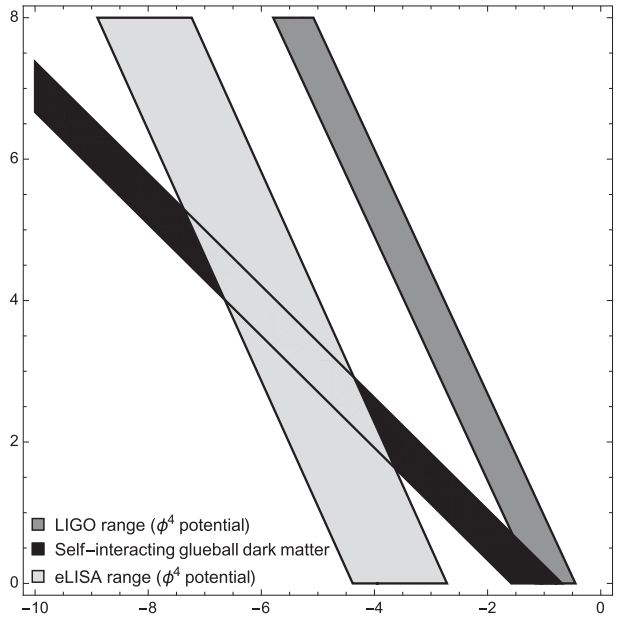

FIG. 4. The parameter space of m (GeV) vs N for the self-interacting glueball dark matter, using the ϕ^4 potential, in the $\sigma \to \infty$ GR limit. The gray (light gray) band indicates the highest frequency of gravitational wave radiation that can be detected by the LIGO (eLISA) experiment. The black band regards the ϕ^4 self-interacting glueball dark matter.

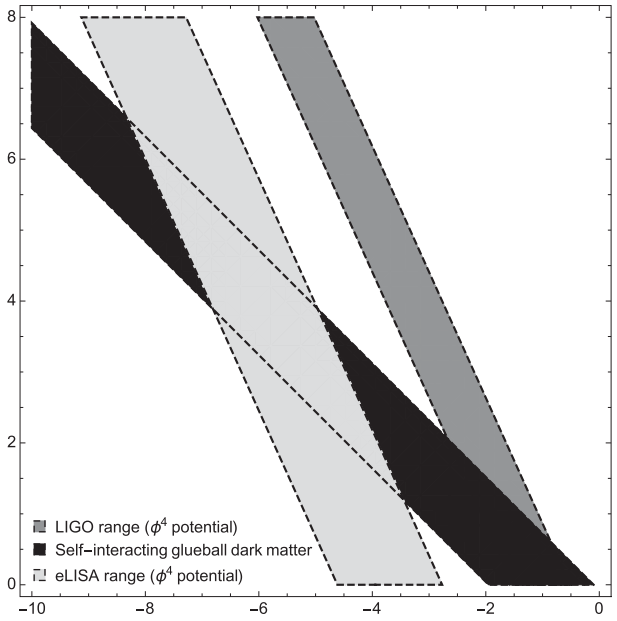

FIG. 5. The parameter space of m (GeV) vs N for the self-interacting glueball dark matter, using the ϕ^4 potential, in the current brane tension bound $\sigma \gtrsim 3.18 \times 10^6$ MeV^4 [21]. The gray (light gray) band indicates the highest frequency of gravitational wave radiation that can be detected by the LIGO (eLISA) experiment. The black band regards the ϕ^4 self-interacting glueball dark matter.

range of gravitational waves frequency 50 Hz $\lesssim f_{\rm max} \lesssim$ 1 KHz, nowadays. Both these ranges are, respectively, represented by the light-gray and the gray bands in Figs. 4 and 5 below, which represent the N-m parameter space. The black band represents the self-interacting ϕ^4 glueball dark matter. Figure 4 is based on the $\sigma \to \infty$ GR limit, whereas Fig. 5 takes into account the brane tension bound $\sigma \gtrsim 3.18 \times 10^6$ MeV^4. The differences between Figs. 4 and 5, both for the ϕ^4 glueball potential, reside on the distinction between the GR limit and the MGD setup, respectively. Although the spectrum of frequencies detected by the LIGO and the eLISA experiments are slightly modified by the 5D Weyl fluid in the MGD setup, when one goes from Fig. 4 to Fig. 5, the self-interacting glueball dark matter (black band) in the N-m parameter space is considerably thickened.

In the next subsection, the glueball potential in the large-N regime shall be employed, to derive similar corrections, due to a fluid brane variable tension.

B. Large number of SU(N) colors

Regarding the large-N limit regime, the scalar glueball potential associated with the SU(N) Yang-Mills dark sector has power counting $\lambda_{i+2} \sim 1/N^i$, where $i \in \mathbb{N}$ for the cubic and higher-order terms in Eq. (10) [14–16]. Considering all higher-order terms, the dark glueball potential (10) in this regime reads [14–16]

$$V(\phi) = \left(\frac{m^2 N}{4\pi}\right)^2 \sum_{i=2}^{\infty} \frac{1}{j!} \left(\frac{4\pi\phi}{Nm}\right)^j, \tag{25}$$

which is the Taylor expansion of the exponential function of the argument $\frac{4\pi\phi}{Nm}$, when its two first terms are not taken into account [16]. Similarly to Eqs. (15)–(17), the coupled equations can be acquired [16,26],

$$\frac{A(\mathrm{x})}{\Omega^2} = {}_2F_1^{-1}(0.5; \{1, 1.5\}; 4\pi\phi^2(\mathrm{x})), \tag{26a}$$

$$\mathrm{M}'(\mathrm{x}) - \mathrm{x}^2 \left(\frac{\Omega^2}{4A(x)}\phi^2(\mathrm{x}) + \frac{\mathcal{I}_0}{16\pi^2}\right) = 0, \tag{26b}$$

$$\frac{(\ln A(\mathrm{x}))'}{B(\mathrm{x})} - \frac{2\mathrm{M}(\mathrm{x})}{\mathrm{x}^2} - \frac{\Omega^2 \mathrm{x}}{2A(\mathrm{x})}\phi^2(\mathrm{x}) + \frac{\mathrm{x}\mathcal{I}_0}{8\pi^2} = 0, \tag{26c}$$

where $\mathcal{I}_0 = \mathrm{I}_0(\phi(\mathrm{x}) - 1)$, and the $\Lambda \gg 1$ regime is adopted [16,26]. The symbol ${}_2F_1$ is the usual generalized hypergeometric function, and I_0 denotes the (modified) Bessel function. These two functions are derived when the time averaging of the potential (25) is computed [16].

The results obtained from using the large-N limit glueball potential in Eq. (25) are plotted in Figs. 6–8. Figures 6–8 take into account finite brane tensions, being smoother than their respective $\sigma \to \infty$ counterparts [16]. Comparing Figs. 1, 2, and 3 (the ϕ^4 dark glueball potential)

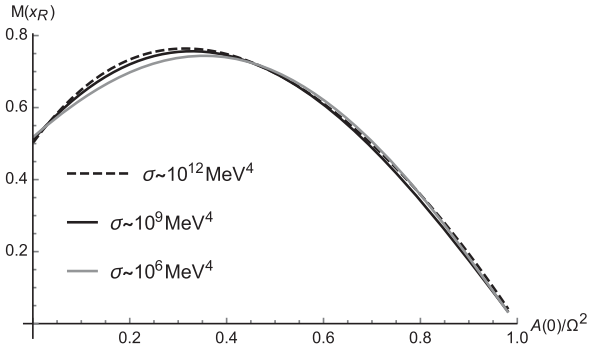

FIG. 6. Dark SU(N) MGD star mass M(x_R), in the scalar glueball potential (25), normalized by $\frac{\sqrt{2\lambda}M_{\rm pl}^3}{m^2}$, with respect to $\frac{A(0)}{\Omega^2}$, for different values of the fluid brane tension $\sigma = 10^{12}$ MeV^4 (dashed line), $\sigma = 10^9$ MeV^4 (black line), and $\sigma \sim 10^6$ MeV^4 (gray line).

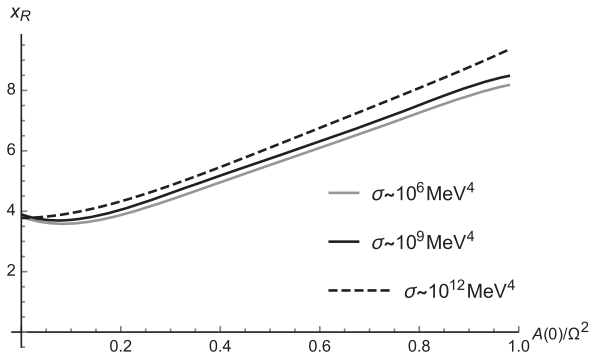

FIG. 7. Dark SU(N) MGD star radius x_R, in the scalar glueball potential (25), normalized by $\frac{\sqrt{2\lambda}M_{\rm pl}}{m^2}$, with respect to $\frac{A(0)}{\Omega^2}$, for different values of the fluid brane tension $\sigma = 10^{12}$ MeV^4 (dashed line), $\sigma = 10^9$ MeV^4 (black line), and $\sigma \sim 10^6$ MeV^4 (gray line).

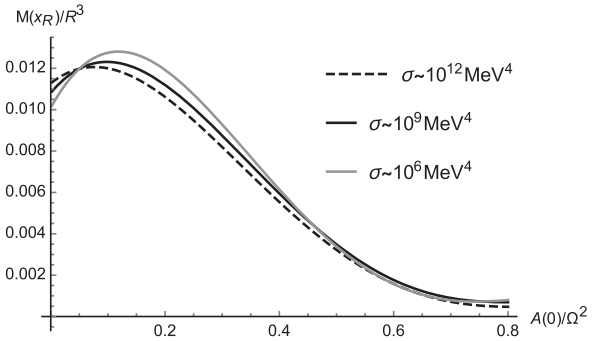

FIG. 8. Dark SU(N) MGD star ration $\frac{\rm M(x_R)}{x_R^3}$, in the scalar glueball potential (25), normalized by $\frac{\sqrt{2\lambda}M_{\rm pl}}{m^2}$, with respect to $\frac{A(0)}{\Omega^2}$, for different values of the fluid brane tension $\sigma = 10^{12}$ MeV^4 (dashed line), $\sigma = 10^9$ MeV^4 (black line), and $\sigma \sim 10^6$ MeV^4 (gray line).

TABLE II. Highest values of the dark SU(N) MGD star radius (normalized by $\frac{\sqrt{2\lambda}}{m^2}M_{\rm pl}$) and mass (normalized by $\frac{\sqrt{2\lambda}}{m^2}M_{\rm pl}^3$), by accretion, for different values of the fluid brane tension, for a the scalar glueball potential (25).

Brane tension σ	$\frac{A(0)}{\Omega^2}$	Mass M(x_R)	Radius x_R	$\frac{\rm M(x_R)}{x_R^3}$
∞ (GR limit)	0.319	0.74	4.7	0.0070
10^{12} (MeV^4)	0.322	0.74	4.9	0.0073
10^9 (MeV^4)	0.327	0.73	4.9	0.0083
10^6 (MeV^4)	0.372	0.72	5.0	0.0084

to, respectively, Figs. 4, 5, and 6 (the large-N limit dark glueball potential), one realizes that the dark SU(N) MGD stars have bigger radii and are more massive that their GR limit counterparts.

Analogously to the self-interacting ϕ^4 glueball potential, in Fig. 6, the mass spectrum (y axis) between the point $\frac{A(0)}{\Omega^2} = 0$ up to the critical (maximum) point in the plots cannot be attained, and a dark SU(N) star accretes and increases its mass up to a maximum, represented in the third column in Table II. The results are presented for different values of the brane tension.

Table II shows that the ratio $\frac{\rm x_R}{\rm M(x_R)}$ is always greater than 2 (in normalized units), irrespectively of the brane tension values, whatever the glueball potential is considered. It means that the radius of a dark SU(N) MGD star is always larger than a Schwarzschild black hole event horizon of same mass, a result similar to the one in Ref. [16] that considers the $\sigma \to \infty$ GR limit. Hence, there is no collapse process of a dark SU(N) MGD star that originates a black hole. The highest frequency of the gravitational wave radiation is again obtained for the maximum value of the dark SU(N) MGD star mass. Both the MGD star highest effective radius and mass, respectively, $R = \frac{1}{2\sqrt{\pi}}\frac{M_{\rm pl}}{Nm^2}x_R$ and $M = \frac{1}{2\sqrt{\pi}}\frac{M_{\rm pl}^3}{Nm^2}\rm M(x_R)$, are presented:

$$R = \begin{cases} \frac{3.57}{Nm^2}, & \text{for } \sigma \to \infty \text{ (GR limit)} \\ \frac{3.72}{Nm^2}, & \text{for } \sigma = 10^{12} \text{ MeV}^4 \\ \frac{3.72}{Nm^2}, & \text{for } \sigma = 10^9 \text{ MeV}^4 \\ \frac{3.79}{Nm^2}, & \text{for } \sigma \sim 10^6 \text{ MeV}^4 \end{cases} \quad (27)$$

$$M = \begin{cases} \frac{0.36}{Nm^2}M_\odot, & \text{for } \sigma \to \infty \text{ (GR limit)} \\ \frac{0.36}{Nm^2}M_\odot, & \text{for } \sigma = 10^{12} \text{ MeV}^4 \\ \frac{0.35}{Nm^2}M_\odot, & \text{for } \sigma = 10^9 \text{ MeV}^4 \\ \frac{0.34}{Nm^2}M_\odot, & \text{for } \sigma \sim 10^6 \text{ MeV}^4 \end{cases} . \quad (28)$$

One then gets a highest gravitational wave frequency, which reads

$$f_{\max} = \frac{m^2 N}{\sqrt{\pi} M_{\rm pl}} \mathrm{supp}^{\frac{1}{2}}\left(\frac{\mathrm{M}(x_R)}{x_R^3}\right) \approx \beta_2(\sigma)\ (50\ \mathrm{Hz}), \tag{29}$$

where the function

$$\beta_2(\sigma) \approxeq 123.4\mathfrak{c}\ (m^2 N)\ \mathrm{GeV}^{-2} \tag{30}$$

has a tuning factor $\mathfrak{c}$, which is a function of the variable brane tension, according to Eq. (29) and to the last column of Table II, given by

$$\mathfrak{c} = \begin{cases} 1, & \text{for } \sigma \to \infty \text{ (GR limit)} \\ 1.020, & \text{for } \sigma = 10^{12}\ \mathrm{MeV}^4, \\ 1.088, & \text{for } \sigma = 10^{9}\ \mathrm{MeV}^4, \\ 1.114, & \text{for } \sigma \sim 10^{6}\ \mathrm{MeV}^4. \end{cases} \tag{31}$$

The parameter $\mathfrak{c}$ indicates the corrections to the unit (that corresponds to the $\sigma \to \infty$ GR limit), for different values for the brane tension.

Similarly to what was accomplished in the Sec. III.A, dark $\mathrm{SU}(N)$ stars have parameters in the ranges $100\ \mathrm{eV} \lesssim m \lesssim 10\ \mathrm{KeV}$ and $10^3 \lesssim N \lesssim 10^6$, yielding a maximum $10^6\ M_\odot \lesssim M \lesssim 10^9\ M_\odot$ for the dark $\mathrm{SU}(N)$ MGD star mass, whereas the lowest dark $\mathrm{SU}(N)$ MGD star radius lies in the range $10^2 \lesssim R \lesssim 10^5$. Hence, the highest frequency of the gravitational wave by dark $\mathrm{SU}(N)$ MGD star mergers is ruled by Eqs. (29) for the large-N limit glueball potential.

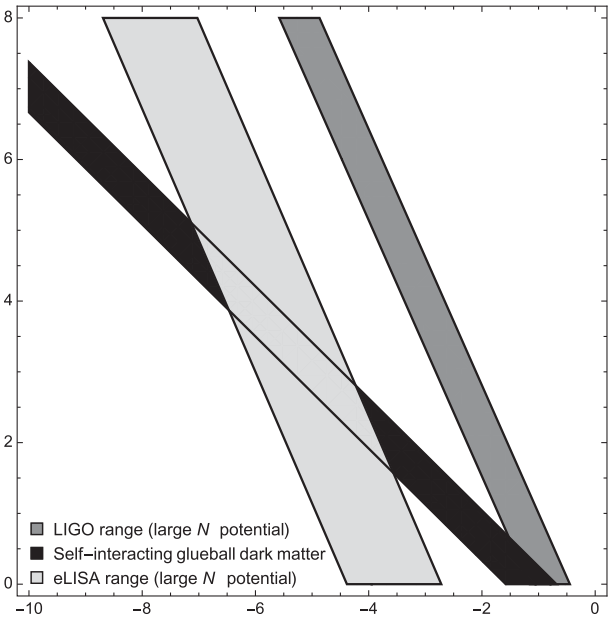

FIG. 9. The parameter space of m (GeV) vs N for the self-interacting glueball dark matter, using the large-N potential, in the $\sigma \to \infty$ GR limit. The gray (light gray) band indicates the highest frequency of gravitational wave radiation that can be detected by the LIGO (eLISA) experiment. The black band regards the large-N self-interacting glueball dark matter.

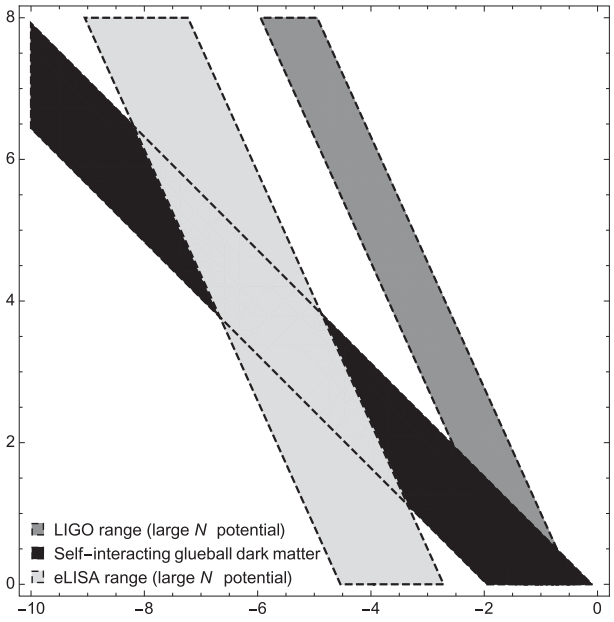

FIG. 10. The parameter space of m (GeV) vs N for the self-interacting glueball dark matter, using the large-N potential, in the current brane tension bound $\sigma \gtrsim 3.18 \times 10^6\ \mathrm{MeV}^4$ [21]. The gray (light gray) band indicates the highest frequency of gravitational wave radiation that can be detected by the LIGO (eLISA) experiment. The black band regards the large-N self-interacting glueball dark matter.

The highest frequency of gravitational wave radiation $f_{\max}$, from dark $\mathrm{SU}(N)$ MGD stellar mergers, can be allocated in the range $30\ \mu\mathrm{Hz} \lesssim f_{\max} \lesssim 100$ mHz, which can be further detected by the eLISA mission [29]. Also, the LIGO experiment can probe the spectrum $50\ \mathrm{Hz} \lesssim f_{\max} \lesssim 1$ KHz. Both these spectra are, respectively, represented by the light gray and the gray bands in Figs. 9 and 10 below, respectively, in the $\sigma \to \infty$ GR limit and in the brane tension bound $\sigma \gtrsim 3.18 \times 10^6\ \mathrm{MeV}^4$, for the large-$N$ glueball potential.

Similarly to the case analyzed in Sec. III. A, the $\sigma \to \infty$ GR limit has a tiny intersection between the possibility of detection at the LIGO experiment and the black band that represents the self-interacting glueball dark matter, in Fig. 9. However, the finite brane tension makes this black band larger in Fig. 10. It represents increased spectra to be probed by the LIGO and eLISA experiments, which are themselves also slightly thickened by braneworld effects. It can be realized by comparing the gray and the light gray bands in Figs. 9 and 10.

IV. CONCLUDING REMARKS AND OUTLOOK

The pure $\mathrm{SU}(N)$ Yang-Mills glueball dark matter model was proposed to condense into dark $\mathrm{SU}(N)$ MGD stars on fluid branes, representing compact configurations of scalar glueball fields. The scalar glueball dark matter model may, eventually, decay into Standard Model elementary particles [14]. Figures 5 and 10 show that a fluid braneworld

scenario, wherein the brane tension varies according to Eq. (8), provides a thickened band that represents the self-interacting glueball dark matter, for, respectively, both ϕ^4 and the large-N potentials that describe the glueball self-interaction. Since by self-interaction the glueballs can agglutinate and condense into dark SU(N) MGD stars, this band has a larger intersection with the LIGO (and the eLISA) experiment to detect gravitational waves.

Taking into account a finite brane tension makes the signature of dark SU(N) star mergers more susceptible to be detected by the LIGO experiment and by the future LISA/eLISA project. In fact, with the most recent and precise brane tension bound [21], Fig. 5 shows a bigger area of intersection, between the self-interacting ϕ^4 glueball dark matter and both the experimental windows for detection, than its GR $\sigma \to \infty$ limit depicted in Fig. 4. Analogously, for the large-N potential, Fig. 10 also presents a larger range of intersection, between the large-N self-interacting potential glueball dark matter and both the LIGO and the eLISA detectable spectra. To summarize, Figs. 4 and 9 represent the GR $\sigma \to \infty$ limit for the ϕ^4 and the large-N potentials that describe the glueball self-interaction, representing a more improbable scenario to detect gravitational waves. Hence, dark SU(N) MGD stars, that have mass and radius corrected by the bulk 5D Weyl fluid, should be better detectable by the current LIGO experiment [25] and by the eLISA project [29].

Finally, the search for TeV-scale gravity signatures in the ATLAS detector at $s = 13$ TeV is being currently approached [30]. Black holes produced with a mass above the formation threshold evaporate in Higgs particles, leptons, particle jets, and photons and are currently searched for at the LHC. Moreover, signatures of TeV extra-dimensional models are encoded in the partners of the Z and W bosons that might be permitted to access the 5D bulk. These partners can be manifested as resonances in dilepton spectra and are more difficult to be detected at the LHC. Kaluza-Klein partners of the Standard Model particles have still not been observed, pushing the lower mass limits beyond 13 TeV. To summarize, collider data indicate string theory magnitude extra dimensions, the searches of which continue at the LHC, and confirmation could happen in the next generation of colliders [31]. The search for evidences of extra dimensions can be, then, dislocated also to observational aspects, as accomplished in Sec. III, by investigating models of which the signatures increase the spectrum of the highest frequency of gravitational wave radiation by the LIGO and eLISA experiments.

ACKNOWLEDGMENTS

R. d. R. is grateful to CNPq (Grant No. 303293/2015-2) and to FAPESP (Grant No. 2015/10270-0) for partial financial support.

[1] J. Ovalle, Int. J. Mod. Phys. D **18**, 837 (2009).
[2] R. Casadio and J. Ovalle, Gen. Relativ. Gravit. **46**, 1669 (2014).
[3] J. Ovalle, L. Gergely, and R. Casadio, Classical Quantum Gravity **32**, 045015 (2015).
[4] R. Maartens and K. Koyama, Living Rev. Relativ. **13**, 5 (2010).
[5] I. Antoniadis, N. Arkani-Hamed, S. Dimopoulos, and G. R. Dvali, Phys. Lett. B **436**, 257 (1998).
[6] C. Germani and R. Maartens, Phys. Rev. D **64**, 124010 (2001).
[7] L. A. Gergely, Phys. Rev. D **79**, 086007 (2009).
[8] R. Casadio, J. Ovalle, and R. da Rocha, Classical Quantum Gravity **31**, 045016 (2014).
[9] L. Randall and R. Sundrum, Phys. Rev. Lett. **83**, 3370 (1999).
[10] T. Shiromizu, K. i. Maeda, and M. Sasaki, Phys. Rev. D **62**, 024012 (2000).
[11] J. Ovalle, Mod. Phys. Lett. A **23**, 3247 (2008).
[12] R. T. Cavalcanti, A. Goncalves da Silva, and R. da Rocha, Classical Quantum Gravity **33**, 215007 (2016).
[13] R. Casadio, J. Ovalle, and R. da Rocha, Europhys. Lett. **110**, 40003 (2015).
[14] J. E. Juknevich, D. Melnikov, and M. J. Strassler, J. High Energy Phys. 07 (2009) 055.
[15] L. Forestell, D. E. Morrissey, and K. Sigurdson, arXiv:1605.08048.
[16] A. Soni and Y. Zhang, Phys. Rev. D **93**, 115025 (2016).
[17] K. K. Boddy, J. L. Feng, M. Kaplinghat, and T. M. P. Tait, Phys. Rev. D **89**, 115017 (2014).
[18] A. S. Miranda, C. A. Ballon Bayona, H. Boschi-Filho, and N. R. F. Braga, J. High Energy Phys. 11 (2009) 119.
[19] J. Ovalle and F. Linares, Phys. Rev. D **88**, 104026 (2013).
[20] M. C. B. Abdalla, J. M. Hoff da Silva, and R. da Rocha, Phys. Rev. D **80**, 046003 (2009).
[21] R. Casadio and R. da Rocha, Phys. Lett. B **763**, 434 (2016).
[22] K. C. Wong, K. S. Cheng, and T. Harko, Eur. Phys. J. C **68**, 241 (2010).
[23] J. Halverson, B. D. Nelson, and F. Ruehle, arXiv: 1609.02151.
[24] L. Barosi, F. A. Brito, and A. R. Queiroz, J. High Energy Phys. 04 (2009) 030.

[25] B. P. Abbott *et al.* (LIGO Scientific Collaboration), Rep. Prog. Phys. **72**, 076901 (2009).
[26] A. Soni and Y. Zhang, arXiv:1610.06931.
[27] M. Colpi, S. L. Shapiro, and I. Wasserman, Phys. Rev. Lett. **57**, 2485 (1986).
[28] M. Gleiser and D. Sowinski, Phys. Lett. B **727**, 272 (2013).
[29] P. A. Seoane *et al.* (eLISA Collaboration), arXiv:1305.5720.
[30] M. Aaboud *et al.* (ATLAS Collaboration), Phys. Lett. B **760**, 520 (2016).
[31] N. Deutschmann, T. Flacke, and J. S. Kim, arXiv:1702.00410.